DEFORMATION PROCESSES IN COMPOSITES PREFORMS

L. Grauers[1], M. Szpieg[1], M. Wysocki[1*], S. Toll[2]

[1] *Swerea SICOMP AB, PO Box 104, SE-431 22 Mölndal, Sweden*
[2] *KTH Royal Institute of Technology, SE-100 44 Stockholm, Sweden*
**maciej.wysocki@swerea.se*

Keywords: *composites performs, Kawabata, hypoplasticity, triaxial testing equipment*

Abstract
The work concerns the inelastic response of composite preforms when subjected to large deformations. The Kawabata equipment has been used to measure the shear and bending properties of the textile reinforcements. In addition, the newly developed triaxial rheometer for out-of-plane shear and compression testing is presented and used. The triaxial rheometer is capable of simultaneous compression and two independent shear deformation modes, allowing for triaxial deformation states. Compared to previous techniques the main benefits are triaxiality, elimination of edge effects and suitability for anisotropic materials. Also, a constitutive theory for the modelling of a wide range of fibrous performs based on hypoplasticity is also presented. The experimental results indicates that even dry preforms behaves viscoelastoplastic as well as showing unsymmetrical behaviour in bending.

1 Introduction

To date, the development and use of textile fibre reinforced polymer composites for lightweight structures has become more and more important. Although all fibre reinforcement is produced as continuous fibre yarns, this is often not the form in which it is finally used in high performance applications. Common textile composites classified according to the fibre architecture include braided, woven, knitted, stitch, bonded and non-woven [1]. Advantages of textile composites include higher strength-to-weight ratios, better impact resistance, better vibration damping properties and higher flexibility. Textile fibre composites are cost effective replacements for pre-impregnated (pre-preg) based laminated composites due to lower manufacturing costs and near net shape production.

Nowadays, the aerospace industry relies on textile reinforcement for use in advanced composites. Due to the high strength, thermal and electrical insulating properties, and fire resistance of some of the man-made fibres, today's commercial aircraft industry uses textiles in the design and manufacture of interior panelling systems, secondary structures (wing-to-body or belly fairing, leading edges, parts and flight control systems) and engine. Manufacturing of composite components usually includes several steps, i.e. cutting the reinforcement, preforming, impregnation of dry preform and curing. Preforming of the dry reinforcement plays a key role in terms of the subsequent manufacturing and the performance of the final product [2].

During a manufacturing operation a preform can be subjected to bending, in and out-of-plane shearing, compacting or combination of these above loadings. Hence, for accurate process simulation of a composite material, it is essential to characterise all the mechanical responses

of the reinforcement itself. The input data from the reinforcement may be then employed in subsequent composite simulations. The understanding of mechanical properties of composites preforms is important for composite manufacturing, and a fair amount of work has gone into analysing these properties [3]. However, previous work on this topic has been limited to simple deformation modes and a restrictive choice of deformation mechanism. Another obstacle were the experimental methods incapable of characterising other than simple deformation modes.

This contribution concerns the inelastic response of composites preforms when subjected to large deformations. The work embraces the experimental as well as the theoretical problems involved. The Kawabata equipment (**KES**) is used for the careful measurement of stress-strain relations. In addition, we describe here the newly developed triaxial rheometer for out-of-plane shear and compression testing [4]. Also, a constitutive theory for the modelling of a wide range of fibrous performs based on hypoplasticity is also presented. The present development is an extension of a previous isotropic model presented in [5]. Finally, selected results from experiments are presented and discussed.

2 Experimental

2.1 Materials

Two different types of carbon fibre textile reinforcements are used. The first one, quasi-UD HexForce® G1157 D 1300 E01 2F, consists of HTA 5131 6K unidirectional carbon fibres in warp direction, and EC9 34Z40 1383 glass fibres in weft direction [6]. The second type of material is a twill weave HexForce® 48302 X 1270 S E01 2F, which consists of AS7 GS 12K carbon fibres both in warp and weft directions [7]. Both of the reinforcing textiles are presented in Fig. 1.

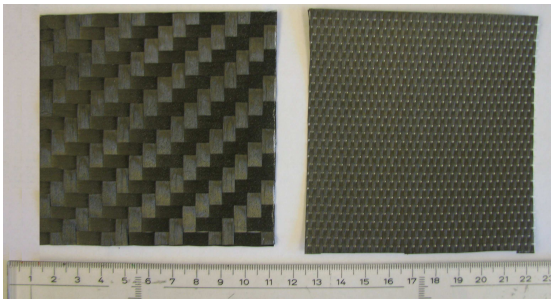

Figure 1. Twill weave and quasi-UD reinforcements.

2.2 Bending

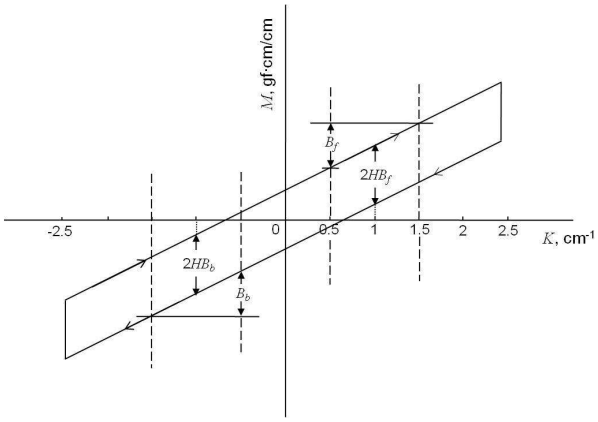

Figure 2. The parameters determined from the bending test for a principal cycle.

Using the KES the bending rigidity and the hysteresis of the bending moment can be determined, per unit sample width. The sample is bent to the maximum curvature of 2.5 cm^{-1} in each direction. The moment is recorded as a function of the curvature. The bending rate is 0.5 cm^{-1}/s. Normally, the width of the samples are 20 cm, however since the tested material has much higher bending stiffness than fabrics, it was necessary to modify the sample size. For the bending along the fibre direction, the samples used had a width of 1 cm and for the bending transverse to the fibre direction the samples had a width of 10 cm.
The bending rigidity for the face side of the sample, B_F, is measured between a curvature of 0.5 and 1.5 cm^{-1}, as indicated in Fig. 2. In the same way but for loading in the opposite direction, the bending rigidity for the back side of the sample, B_B, is obtained between a curvature of -0.5 and -1.5 cm^{-1}. The value of the bending rigidity, B, for a certain cycle is the mean value of B_F and B_B. The hysteresis of the bending moment, $2HB$, for a cycle is the mean value of $2HB_F$ and $2HB_B$, measured at 1 and -1 cm^{-1}, respectively, as indicated in Fig. 2. The sensitivity on KES was set to the option 2x1 for all the bending measurements and the equipment was calibrated before performing the first bending test.For each sample three bending cycles have been recorded; the first, fifth and tenth. This was done in order to determine the changes in required moment for bending at increasing cycles. It is possible that the moment could change due to the fact that the binder breakage during the first cycles.

2.3 Shear
The shear properties of the material have also been characterised using the Kawabata equipment. The shear force F_S as a function of the shear angle φ was recorded and the shearing rigidity per unit sample width has been determined along with the hysteresis of the shear force per unit sample width at 0.5° and 5°. The sample is sheared to an angle $\varphi = \pm 8°$. The force perpendicular to the shearing is kept constant at 20 gf/cm (around 0.2 N/cm). The sample is sheared with a rate of 0.477°/s. The width of the typical sample is 20 cm as for the bending. For these tests the width of the specimens was reduced to 10 cm, since it is a rigid material compared to textiles. This must be taken into account when analyzing the results. The length of the tested material, i.e. the material between the clamps, is 5 cm.

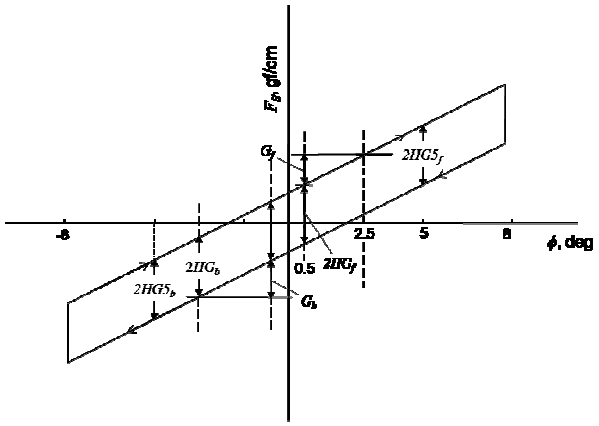

Figure 3. A principal sketch of the shear test performed using the Kawabata equipment.

The shearing rigidity for the face side of the sample, G_F, is obtained as indicated in Fig. 5. The difference in shearing force between a shear in angle of 0.5 and 2.5° is divided by the angle interval, i.e. 2°. In the same way but for loading in the opposite direction, the bending rigidity for the back side of the sample, G_B, is obtained between -0.5 and -2.5°. The value of G for a certain cycle is the mean value of G_F and G_B for that cycle. The hysteresis of the shearing force per unit sample width, $2HG_F$ and $2HG5_F$, are determined at 0.5° and 5°,

respectively. For the loading in the other direction, the hysteresis is determined at -0.5 and -5°. For each cycle the mean value of $2HG_F$ and $2HG_B$ gives *2HG* and the mean of $2HG5_F$ and $2HG5_B$ gives *2HG5*. Similarly to the bending test, three cycles have been recorded for each test; the first, fifth and tenth cycle.

2.4 Triaxial rheometer

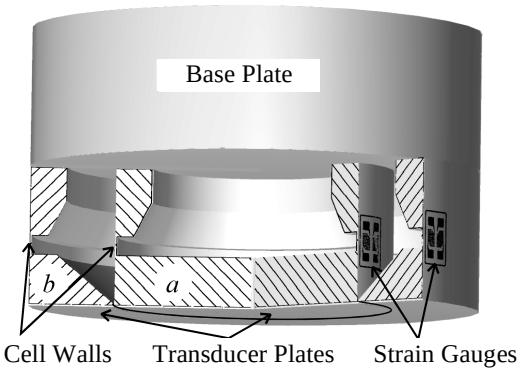

Figure 4. Section of the transducer head.

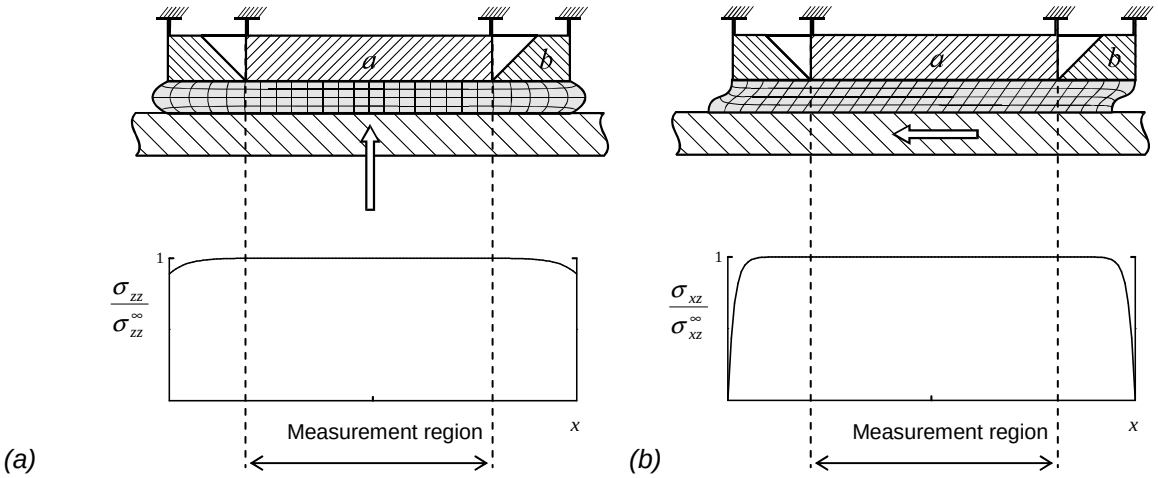

Figure 5. Schematic of sample deformation and (a) the resulting stress distribution $\sigma_{zz}(x)$ in compression and (b) the resulting stress distribution $\sigma_{xz}(x)$ in shear. The arrows indicate the relative motion of the plates.

The triaxial rheometer instrument used here consists of a frame, a ball screw driven x,y,z-table, a specially designed triaxial stress transducer head. The sample is fixed between the transducer head and the x,y,z-table, acting as the upper and the lower plate, respectively. The relative position between the upper and lower plate and the x- and y-directions are measured discretely by on-board linear scales with a resolution of 0.1 μm. The resolution of the stress transducer is about 10 Pa in compression and 1 Pa in shear. The development of the key component of the apparatus, the transducer head, was described in [4] and is depicted in Fig. 4. Two concentric transducer plates, *a* and *b*, are attached to a base plate via triaxial load cells. The chief purpose of this arrangement is to absorb the free edge effect at transducer *b* and thus measure the true material stress response at transducer a. Fig. 5 illustrates the stress

distribution in compression and shear. In consequence, if the sample is sufficiently thin, the stress distribution underneath transducer *a* will be uniform and the measurement will represent the true stress response of the material.

2 Model development

A constitutive theory aimed for modelling of a wide range of fibrous preforms based on hypoplasticity is under development. The present work is extension of the isotropic model in [5]. Based on the work in [5], we introduce a stress energy function and derive a dissipation inequality in terms of the stress dependent operators of the transverse isotropic hypoplastic law. A general form for the nonlinear operator is also found, and implemented for numerical studies. In particular, the material is assumed to have transversely isotropic symmetry with a director **n**. We define two partial stress tensors: a conservative, hyperelastic, stress $\boldsymbol{\tau}_e$ and a non-conservative stress $\boldsymbol{\tau}_*$,

$$\boldsymbol{\sigma} = \boldsymbol{\tau}_e + \boldsymbol{\tau}_*, \tag{1}$$

where $\boldsymbol{\sigma}$ is the Cauchy stress. The conservative stress is assumed to be a function of the deformation, while the non-conservative stress governed by an evolution law:

$$\boldsymbol{\tau}_e = \mathcal{F}\left(\phi, \lambda, \mathbf{F}, \mathbf{n}_0\right), \tag{2}$$

$$\dot{\boldsymbol{\tau}}_* = \mathcal{G}\left(\phi, \boldsymbol{\tau}_*, \mathbf{l}, \mathbf{n}\right) + \boldsymbol{\omega}\boldsymbol{\tau}_* - \boldsymbol{\tau}_*\boldsymbol{\omega}\,, \tag{3}$$

where

$$\boldsymbol{\omega} = \mathbf{w} + \mathbf{dnn} - \mathbf{ndn}\,, \tag{4}$$

here ϕ is the fibre volume fraction, λ is the fibre stretch, **F** is the deformation gradient, **l** is the velocity gradient, with symmetric and skew symmetric parts **d** and **w**. The objectivity of the evolution law (3) may be verified in the usual way.

The conservative stress $\boldsymbol{\tau}_e$ may be developed using standard hyperelasticity [2] and will not be dwelled on here. The constitutive models for the non-conservative stress, on the other hand, are developed by introducing a free energy per unit reference volume in terms of stress invariants as:

$$\Psi_* = \frac{1}{2}\phi^{-n}\left(\frac{j_4}{C_L} + \frac{j_5}{C_T}\right), \tag{5}$$

where C_L and C_T are the longitudinal and transverse shear moduli, respectively, and stress invariants defined in a similar way to the transverse isotropic hyperelastic strain invariants:

$$j_4 = \mathbf{n}\cdot\boldsymbol{\tau}_*^2\cdot\mathbf{n} \text{ and } j_5 = \frac{1}{2}\mathbf{1}:\boldsymbol{\tau}_*^2 - \mathbf{n}\cdot\boldsymbol{\tau}_*^2\cdot\mathbf{n}\,. \tag{6}$$

It may further be proved that the operator $\mathcal{G}\left(\phi, \boldsymbol{\tau}_*, \mathbf{l}, \mathbf{n}\right)$, may be partitioned into a transversely isotropic fourth order linear operator $\mathcal{L}\left(\phi, \mathbf{n}\right)$ and a scalar dissipation function $\mathcal{R}\left(\phi, \boldsymbol{\tau}_*, \mathbf{d}, \mathbf{n}\right)$. Moreover, taking into consideration (5) and (6), the linear operator becomes

$$\begin{aligned}\mathcal{L}(\phi,\mathbf{n}) = \phi^n \big[& C_L \left(\mathbf{1} \overline{\otimes} \mathbf{1} + \mathbf{1} \underline{\otimes} \mathbf{1} - \mathbf{1} \otimes \mathbf{1} + \mathbf{1} \otimes \mathbf{nn} + \mathbf{nn} \otimes \mathbf{1} \right) \\ & \left(C_L - C_T \right) \left(\mathbf{1} \overline{\otimes} \mathbf{nn} + \mathbf{1} \underline{\otimes} \mathbf{nn} + \mathbf{nn} \underline{\otimes} \mathbf{1} + \mathbf{nn} \overline{\otimes} \mathbf{1} \right) \\ & - \left(4C_L - C_T \right) \mathbf{nnnn} \big] \end{aligned} \quad . \tag{7}$$

For the dissipation function we may assumed the Coulomb type behaviour

$$\varsigma = \frac{\phi^{-n}}{kE_f} \sqrt{\frac{j_4}{\mu_4^2} + \frac{j_5}{\mu_5^2}} \tag{8}$$

and consider the form

$$\mathcal{R}(\phi, \boldsymbol{\tau}_*, \mathbf{d}, \mathbf{n}) = \mathcal{Z}\left(\nabla\varsigma : \mathcal{L} : \mathbf{d} \right) + \frac{1}{2}(n+1)\mathcal{Z}\left(\mathbf{1} : \mathbf{d} \right), \tag{9}$$

where $\nabla\varsigma = \partial\varsigma / \partial\boldsymbol{\sigma}_*$ and $\mathcal{Z}$ is a form of Heaviside function; in principle equal to its argument if the latter is positive and zero otherwise. In particular, the argument of the $\mathcal{Z}$-function is the rate of increase of the slip stress function ς due to the elastic stress rate. Finally, differentiation of (9) leads to the following form of the dissipation function

$$\nabla\varsigma : \mathcal{L} : \mathbf{d} = \frac{1}{kE_f} \left(\frac{j_4}{\mu_4^2} + \frac{j_5}{\mu_5^2} \right)^{-\frac{1}{2}} \left[2 \left(\frac{C_L}{\mu_4^2} + \frac{C_T}{\mu_5^2} \right) \mathbf{n} \cdot \boldsymbol{\tau}_* \mathbf{dn} + \frac{C_T}{\mu_5^2} \boldsymbol{\tau}_* \cdot \mathbf{d} \right]. \tag{10}$$

3 Results and discussion

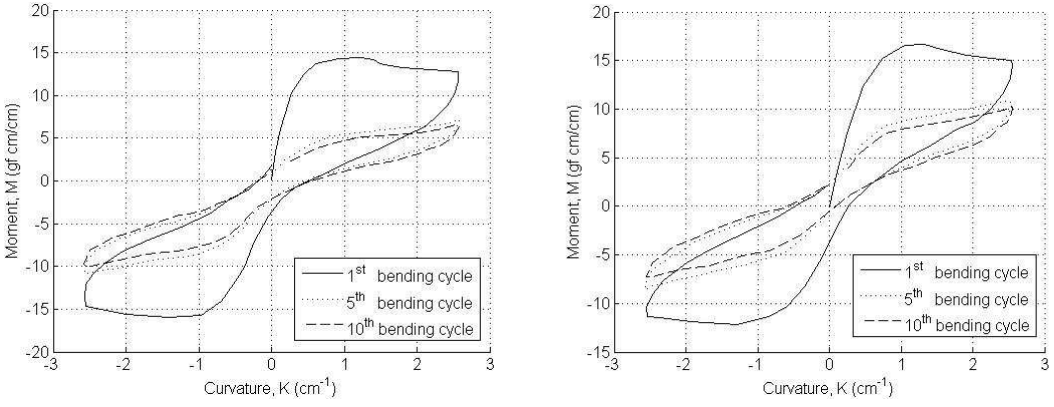

Figure 6. . Representative curves from the bending of the quasi-UD preform transverse to the fibre direction using KES-FB; a) face side bends first, b) back side bends first. NOTE, the scale in both plots is different.

A typical roll of preform has its face side and its back side. Hence, during the measurements, the order of the bending side of the preform is taken into account. This is due to the fact that different amount of binder might me present on each side of the preform, resulting in different values of the bending rigidity, *B*, and hysteresis of bending moment, *2HB*. The representative curves from the bending test of the quasi-UD preforms are presented in Figures 6.

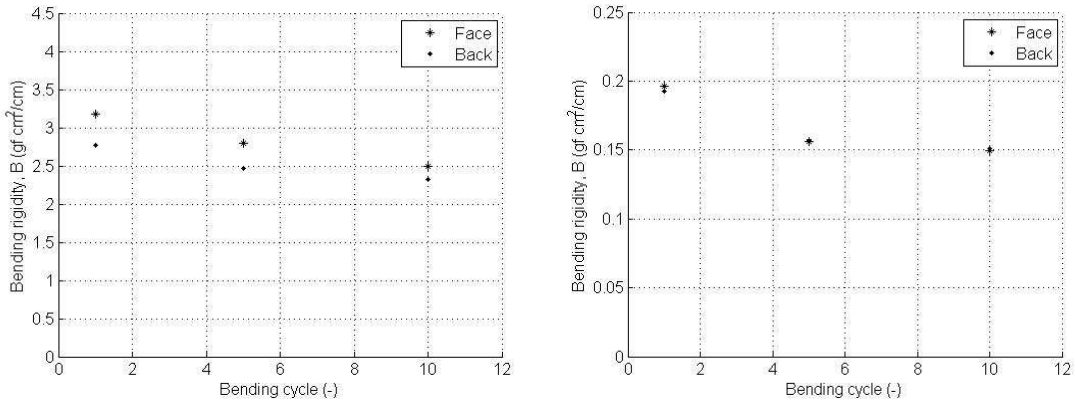

Figure 7. Bending rigidity, *B*, for quasi-UD preform:
a) transverse to the fibre direction, b) along the fibre direction.

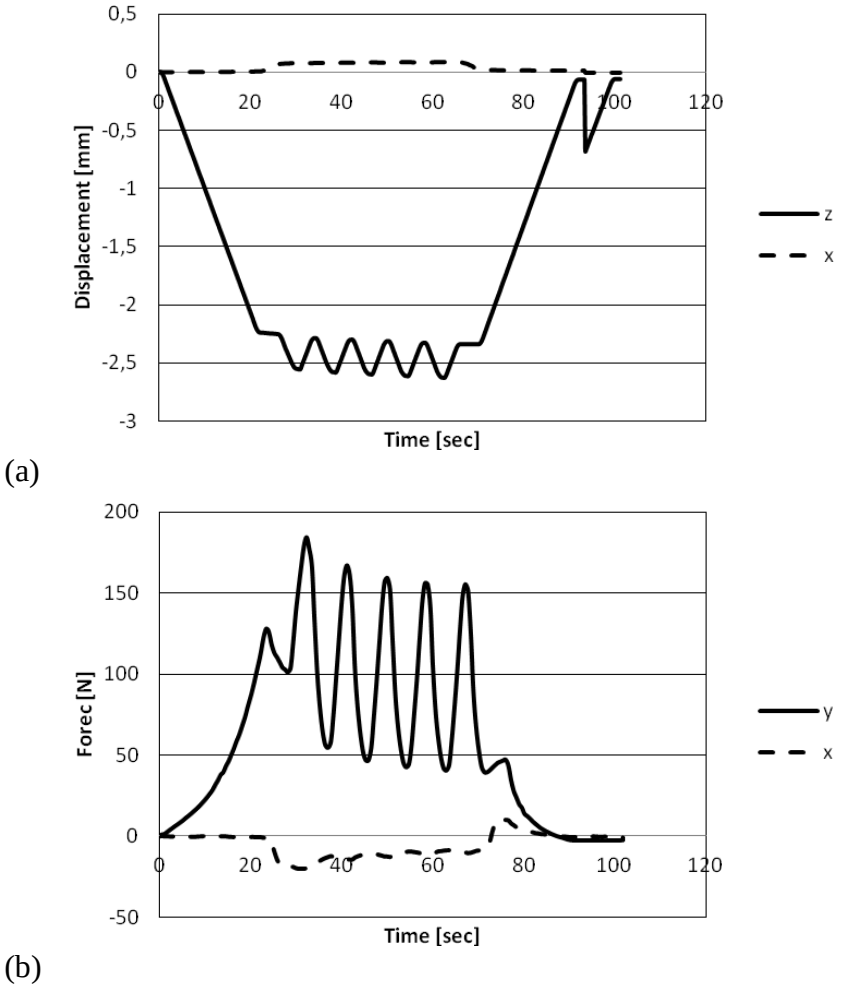

Figure 8. The results from triaxial rheometer of the the quasi-UD preform testing;
(a) excitation profile and (b) the resulting force.

The results in Fig. 7 show the bending rigidity after one, five and ten bending cycles and are the average values from measurements of 10 samples. The subscripts face and back in the legend denote which side of the sample bends first during the measurement. In terms of the

characteristic values (*B* and also *2HB* not shown in this paper), the differences between different sides of the considered preforms are rather minor. However, there is some scatter in the bending rigidity, *B*, of the quasi-UD preform tested transverse to the fibre direction. This may be attributed to a different amount of binder on each side of the preform. The bending rigidity, *B*, is higher for the face side, indicating higher amount of binder present on this particular side of the preform. Another discrepancy can be observed for the hysteresis of bending moment of the twill weave preform during the first bending cycle. This might be attributed to the uneven spreading of binder.

The results from testing of the quasi-UD preform using the triaxial rheometer are presented in Fig. 8. The excitation profile consists of an initial compression in z-direction, followed by shear in x-direction, followed by five cycles of additional compression, and finally return to the reference position by reversing the x and z displacements. The main result is the relaxation of the z-force during both the initial loading, but also during the cyclic z-loading. This indicates that the material behaves viscous. As expected, also the force in x-direction relaxes during the cycling loading in z-direction. During unloading of the x-displacement, the force reverses and becomes negative, indicating dissipative processes within the material. In particular, it appears the in addition to viscous processes also plastic processes develop in this particular preform.

The shearing rigidity and the hysteresis of the shearing force tests where also preformed. However, due to the limited amount of space, the results regarding shear properties of the reinforcing textiles will be omitted here. This is also truth for the assessment of the constitutive model presented here.

References

[1] Horrocks AR, Anand SC. *Handbook of technical textiles*. Woodhead Publishing Limited, ISBN 1 85573 385 4

[2] Wysocki M. *Continuum Modelling of Composites Consolidation*. PhD Thesis, Department of Applied Mechanics, Chalmers University of Technology, Sweden (2006)

[3] Chan CK, Jiang XY, Liew KL, Chan LK, Wong WK, Lau MP. Evaluation of mechanical properties of uniform fabrics in garment manufacturing. *Journal of Materials Processing Technology*, **174**:183-189 (2006)

[4] Alkhagen M. Toll S. A triaxial rheometer for soft compressible solids, *Journal of Rheology* Volume **46**(1), 31-47 (2002)

[5] Toll S. The dissipation inequality in hypoplasticity, Acta Mechanica, **221**(1-2), 39-47 (2011)

[6] HexForce® G1157 D 1300 E01 2F, Quasi-UD Fabric. Technical datasheet, Hexcel®, (2010)

[7] HexForce® 48302 X 1270 S E01 2F, Twill weave. Technical datasheet, Hexcel®, (2010)